

Testing AdS early dark energy with Planck, SPTpol and LSS data

Jun-Qian Jiang^a Yun-Song Piao^{a,b,c,d}

^a*School of Physics, University of Chinese Academy of Sciences, Beijing 100049, China*

^b*School of Fundamental Physics and Mathematical Sciences, Hangzhou Institute for Advanced Study, UCAS, Hangzhou 310024, China*

^c*International Center for Theoretical Physics Asia-Pacific, Beijing/Hangzhou, China*

^d*Institute of Theoretical Physics, Chinese Academy of Sciences, P.O. Box 2735, Beijing 100190, China*

E-mail: jqjiang@zju.edu.cn, yspiao@ucas.ac.cn

ABSTRACT: The Hubble tension might be resolved by injecting a new energy component, called Early Dark Energy (EDE), prior to recombination. An Anti-de Sitter (AdS) phase around recombination can make the injected energy decay faster, which thus allows a higher EDE fraction (so larger H_0) while prevents degrading the CMB fit. In this work, we test the AdS-EDE model with CMB and Large-Scale Structure (LSS) data. Our CMB dataset consists of low- ℓ part of Planck TT spectrum and SPTpol polarization and lensing measurements, since this dataset predicts the CMB lensing effect consistent with Λ CDM expectation. Combining it with BAO and Pantheon data, we find the bestfit values $H_0 = 71.92$ km/s/Mpc and $H_0 = 73.29$ km/s/Mpc without and with the SH0ES prior, respectively. Including cosmic shear and galaxy clusters data, we have $H_0 = 71.87$ km/s/Mpc and $S_8 = 0.785$, i.e. only 1.3σ discrepancy with direct S_8 measurement.

Contents

1	Introduction	1
2	A brief review on AdS-EDE model	3
3	Methodology	4
4	Consistency check of CMB data sets	5
5	Results	7
5.1	Planck_low ℓ + SPT	7
5.2	Planck_low ℓ + SPT + BAO + Pantheon	7
5.3	Planck_low ℓ + SPT + BAO + Pantheon + SH0ES	12
5.4	Planck_low ℓ + SPT + BAO + Pantheon + SH0ES + RSD + WL	12
6	Discussion	14
7	Conclusion	16
A	Results with Planck_lowℓ + SPT + BAO + Pantheon + SH0ES + EFTofLSS	18
B	Results with fullPlanck+BAO+Pantheon	19

1 Introduction

Currently, the Λ CDM model is being confronted with unsolved tensions. One is the H_0 tension, i.e. the discrepancy between the direct and indirect measurements of Hubble constant H_0 [1, 2]. Based on standard Λ CDM model, the Planck collaboration found $H_0 = 67.27 \pm 0.60$ km/s/Mpc [3], see also recent SDSS-IV result [4]. In contrast, using Cepheid-calibrated supernovae, the SH0ES found $H_0 = 74.03 \pm 1.42$ km/s/Mpc [5], which is 4.4σ inconsistent with Planck’s result. Different local measurements (independent of cosmological model) have actually bring similar higher H_0 , which make it unlikely to be blamed on single systematic error. Therefore, the physics beyond Λ CDM model might be required, see e.g.[6–8] for recent reviews.

Another is the S_8 tension, i.e. the discrepancy between CMB and Large-Scale Structure (LSS) observations, which is quantified using $S_8 \equiv \sigma_8 \sqrt{\Omega_m/0.3}$, where σ_8 is the amplitude of matter density fluctuation at low redshift. Based on flat Λ CDM model, the Planck collaboration found $S_8 = 0.834 \pm 0.016$ [3]. However, the weak lensing measurements and redshift surveys prefer lower values, e.g. $S_8 = 0.766^{+0.020}_{-0.014}$ for KiDS-1000+BOSS DR12+2dfLenS [9] and $S_8 = 0.737^{+0.040}_{-0.036}$ for KiDS+VIKING-450 [10], see also [11].

Recently, the Early Dark Energy (EDE) scenario [12, 13] for resolving the H_0 tension has been proposed. In light of the requirement that EDE must be non-negligible only for a short period around matter-radiation equality and before recombination, this early dark component can be modelled as fields with certain phenomenological potentials, such as ultra-light axion-like potential [13, 14], power-law potential [15], also ADE [16], NEDE [17] and CEDE [18]. In particular, it is found in Ref.[19], see also [20], that the existence of an Anti-de Sitter (AdS) phase around recombination can lift H_0 more effectively while less spoil to CMB fit. In past years, the EDE models have been extensively studied [21–31], see also modified gravity models e.g.[32–36].

It has been noticed that the scenarios resolving the Hubble tension will inevitably exacerbate the S_8 tension between CMB and LSS. After adding LSS data, Ref.[37] showed that for ultra-light axion-like EDE, the fraction of EDE is downed to $f_{\text{EDE}} < 0.06$, which makes it impossible to resolve Hubble tension, see also similar results by using Effective Field Theory of Large-Scale Structure (EFTofLSS) [38, 39]. These seems suggest that the EDE is being faced with the significant challenge from LSS observations, see also [40], though it may due to our inappropriate Bayesian analysis method [41, 42]

There are also discords inside CMB datasets. It's well-known that there seems to be inconsistency between the high- ℓ and low- ℓ part in Planck's TT power spectrum [43], where the low- ℓ part favors higher H_0 and lower S_8 . Planck blamed it to the combined effects of an oscillatory-like set of high- ℓ residuals and the deficit in low- ℓ ($\ell < 30$) power [44]. Gravitational lensing effect can smooth sound peaks (mainly affects high- ℓ part), which, however, is stronger than what is expected in Λ CDM model [43, 45]. Generally, one quantifies this effect by A_L , which equals 1 in a self-consistent model, but actually $A_L = 1.180 \pm 0.065$ for Planck [3]. As a contrast, we have not found this over smoothing effect in ground-base CMB observations. Actually, we see $A_L = 1.01 \pm 0.11$ for ACT [46], while $A_L = 0.81 \pm 0.14$ SPTpol [47], which is even lower than expected.

As the CMB observation covering the widest sky area, Planck measures the most precise TT spectrum in low- ℓ part. Ground based CMB observations, such as SPT, ACT and POLARBEAR, focus on the polarization power spectrum at small scale. They can cover higher ℓ than Planck. Therefore, Ref.[48, 49] discarded Planck's high- ℓ part and chose to combine Planck low- ℓ TT power spectrum and SPTpol polarization spectrum to test the EDE model. In this way, the most debatable part of Planck data can be avoided, and interestingly, higher H_0 and lower S_8 are found. See also Ref.[50, 51] for results with ACT DR4 data.

In AdS-EDE model [19], $H_0 > 72$ km/s/Mpc is compatible with direct H_0 measurement at 1σ level. However, it also suffers from the S_8 tension. Using datasets containing full Planck data, BAO, supernova, SHOES data, we found $\sigma_8 = 0.8514$. This larger σ_8 seems inevitable due to the positive correlation between $\Omega_m h^2$ and H_0 [20]. Thus it is significant to revisit the constraining power of LSS on the AdS-EDE model using the different CMB dataset that predicts the consistent CMB lensing effect [48, 49]. Moreover, it is also interesting to estimate the effect of H_0 prior on AdS-EDE model. In this work, we will test AdS-EDE model with combined Planck.low ℓ +SPTpol dataset, as well as LSS data.

The paper is organized as follow. We give a brief review on AdS-EDE model in

section 2. The datasets and methodology are showed in section 3. Then we check the consistency of our CMB dataset in section 4 and present results in section 5. We discuss our result with power spectrum in section 6. And we conclude in section 7.

2 A brief review on AdS-EDE model

It is well-known that the CMB observations measures the angle θ_s^* projected on the last-scattering surface of sound horizon (when the photon decoupled),

$$\theta_s^* = \frac{r_s^*}{D_A^*}, \quad (2.1)$$

where the sound horizon

$$r_s^* \equiv \int_0^{t^*} \frac{dt}{a(t)} c_s(t) = \int_{z_*}^{\infty} \frac{dz}{H(z)} c_s(z) \quad (2.2)$$

with c_s set by the densities of baryons and matter, and the angle distance D_A^* to the last-scattering surface by

$$D_A^* = \int_0^{z_*} \frac{dz}{H(z)} \propto \frac{1}{H_0}. \quad (2.3)$$

Reducing r_s will lift $H_0 \sim 1/r_s$, which can be achieved by injecting certain dark component prior to recombination [52]. The corresponding dark energy is usually called EDE, whose the parameter of state $w \approx -1$ at beginning and hereafter $w > 1/3$ around recombination to dilute faster than radiation.

In string theory, it is easy to construct AdS vacua e.g.[53, 54], which so are ubiquitous. And AdS vacua are also important due to AdS/CFT duality [55]. In contrast, a meta-stable dS vacuum is difficult to construct (i.e belongs to the swampland) [56–58]. See also e.g.[59–61] for the implications of AdS vacua on primordial Universe and e.g.[62–65] for the implications of AdS vacua on the late Universe. Our phenomenological potential modelling AdS-EDE is that in Ref.[19]:

$$V(\phi) = \begin{cases} V_0 \left(\frac{\phi}{M_{\text{Pl}}} \right)^4 - V_{\text{AdS}}, & \frac{\phi}{M_{\text{Pl}}} < \left(\frac{V_{\text{AdS}}}{V_0} \right)^{1/4} \\ 0, & \frac{\phi}{M_{\text{Pl}}} > \left(\frac{V_{\text{AdS}}}{V_0} \right)^{1/4} \end{cases} \quad (2.4)$$

where M_{Pl} is the reduced Planck mass. V_{AdS} is the depth of AdS phase. See Figure 1 for one of the best-fit potential in this work.

At beginning, the field is fixed in a high-energy region of its potential (left part in Figure 1) by Hubble friction. Generally, we have $\rho_\phi = \dot{\phi}^2/2 + V(\phi)$, $P_\phi = \dot{\phi}^2/2 - V(\phi)$ for scalar field, so initially $w \equiv P/\rho \approx -1$, thus the field behaves like the dark energy. And the fraction of EDE raised with the redshift of matter and radiation. When H is decreased to satisfy $\partial_\phi^2 V(\phi) \approx 9H^2$, the field will roll down along its potential to AdS phase $V < 0$, where $w > 1$. Now ρ_{EDE} will redshift as $\rho \propto a^{-3(1+w)}$. After recombination, the field will climb up the other side of the potential and maintains $V = \text{const.} \geq 0$, which might result in accelerated expansion of current Universe. Here we set it to 0.

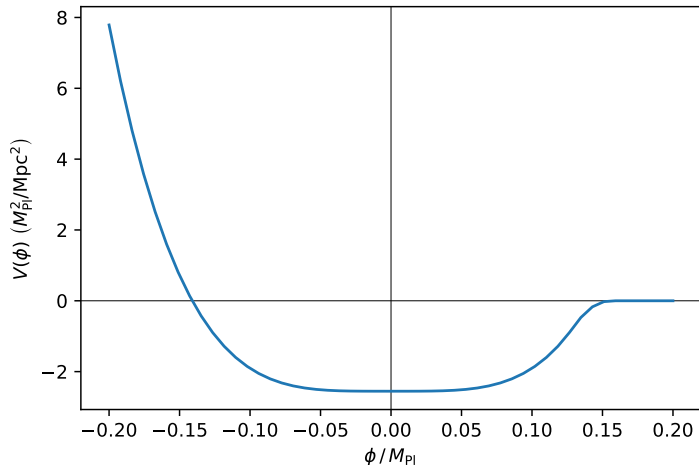


Figure 1. The potential of AdS-EDE with best-fit values to Planck_low ℓ + SPT + BAO + Pantheon + SH0ES. The field frozen at the initial point until $\partial_\phi^2 V(\phi) \approx 9H^2$. Then it will roll through the AdS phase, and arrive at the flat region of potential with $V > 0$ finally.

By decaying in a faster way, AdS-EDE can avoid degrading the CMB fit, which makes higher EDE fraction (so a larger H_0) possible.

3 Methodology

As a phenomenological model [19], besides six parameters of Λ CDM model, we choose $\{\ln(1+z_c), \omega_{\text{scf}}, \alpha_{\text{AdS}}\}$ rather than $\{V_0, V_{\text{AdS}}, \phi_i\}$ as EDE's parameters. z_c is the redshift that satisfy $\partial_\phi^2 V(\phi_c) = 9H_c^2$, i.e. the redshift when EDE field starts to slow roll, ω_{scf} is the physical fraction of EDE, and α_{AdS} is defined by $V_{\text{AdS}} = \alpha_{\text{AdS}} (\rho_m(z_c) + \rho_r(z_c))$.

We modified CLASS v2.9.4 [66] and MontePython v3.4 [67, 68] to run Markov chain Monte Carlo (MCMC) analysis, and convert EDE parameters by shooting algorithm. Non-linear matter power spectrum is calculated by using HALOFIT [69, 70], whose suitability for EDE model is checked in [37]. A large α_{AdS} will cause the field fails to climb up the potential while a small α_{AdS} is just a run-away potential without AdS phase. Thus we will fix it to a value that dose not lead to a collapsing Universe while having a significant AdS phase. We follow [19] and set $\alpha_{\text{AdS}} = 3.79 \times 10^{-4}$. We also adopt the same neutrino assumption as Planck. In addition, since the field in AdS-EDE model does not oscillate and thus cannot be approximated using the fluid approximation, we choose to solve the Klein-Gordon equation directly (see [15] for EDE with power-law potential).

Here, all parameters are assumed with flat prior. The sampling range of $\ln(1+z_c)$ is set as [7.5, 9] to ensure the decaying of EDE before recombination. We also set a very small lower limit for ω_{scf} to avoid the sampling difficulty when ω_{scf} is too small and has too weak constraint power on other EDE parameters.¹ The Gelman-Rubin criterion for

¹In fact, in light of the posterior distribution below, we need not to worry about it.

all chains is converged to $R - 1 < 0.15$. The posterior distribution is analyzed and plotted using `GetDist` [71].

We consider the data sets as follows:

- **Planck_low ℓ** : The TT power spectrum of Planck 2018 [3] at $\ell < 1000$, including $30 \leq \ell < 1000$ part of `Planck` likelihood and $\ell < 30$ part of `Commander` likelihood. All nuisance parameters are imposed with the same prior with Planck.
- **SPTpol**: The polarization power spectrum (TE and EE) measured by 500 deg² SPTpol survey [47]. Their multipole range is $50 < \ell \leq 8000$. Due to very small sky area overlap between SPTpol and Planck, the correlation between them can be ignored. All nuisance parameters are imposed with the same prior with SPTpol.
- **SPTlen**: The CMB lensing potential measured by 500 deg² SPTpol survey [72][73]. Their multipole range is $100 < \ell \leq 2000$. Here, for simplicity, we denote the dataset combination SPTpol + SPTlen as **SPT**.
- **BAO**: low redshift BAO measured by 6DF [74] in $z = 0.106$ and SDSS DR7 MGS [75] in $z = 0.15$, as well as the ‘consensus’ final result from BOSS DR12 combined analysis [76], their effective redshifts are $z = 0.38, 0.51, 0.61$.
- **Pantheon**: We take use of the magnitudes and luminosity distances data of supernovae from Pantheon. [77]
- **SHOES (R19)**: The local H_0 measured with Cepheid-calibrated supernovae by SHOES: $H_0 = 74.03 \pm 1.42$ km/s/Mpc [5], is regarded as a Gaussian prior.
- **RSD**: The ‘consensus’ final result from BOSS DR12 [76]. RSD helps us constraint $f\sigma_8$. When we add RSD data, we also use the BAO data and the covariance of combined BAO+FS analysis.
- **WL**: We directly take use of the constraint to S_8 from the combined analysis of KiDS+VIKING-450 + DES-Y1 dataset, i.e. $S_8 = 0.755^{+0.019}_{-0.021}$ [78] for Λ CDM. In principal, we should use the full likelihood, but as checked in [37], there is little difference in result between a Gaussian prior on S_8 and full likelihood for EDE.

In addition, we include Planck 2018 measurements of the low ℓ part of the EE spectrum ($\ell < 30$) [3] by default in all datasets combinations. This part of data can constrain τ , so as to break the degeneracy of $A_s e^{-2\tau}$.

4 Consistency check of CMB data sets

Our CMB dataset is Planck_low ℓ +SPT, i.e. Planck_low ℓ +SPTpol+SPTlen. Ref.[48] has checked the consistency of this dataset by comparing its posterior distributions under Λ CDM model. However, as we have modified cosmological model, we will have different posterior distributions, some of which may be very different. Therefore, it is required to

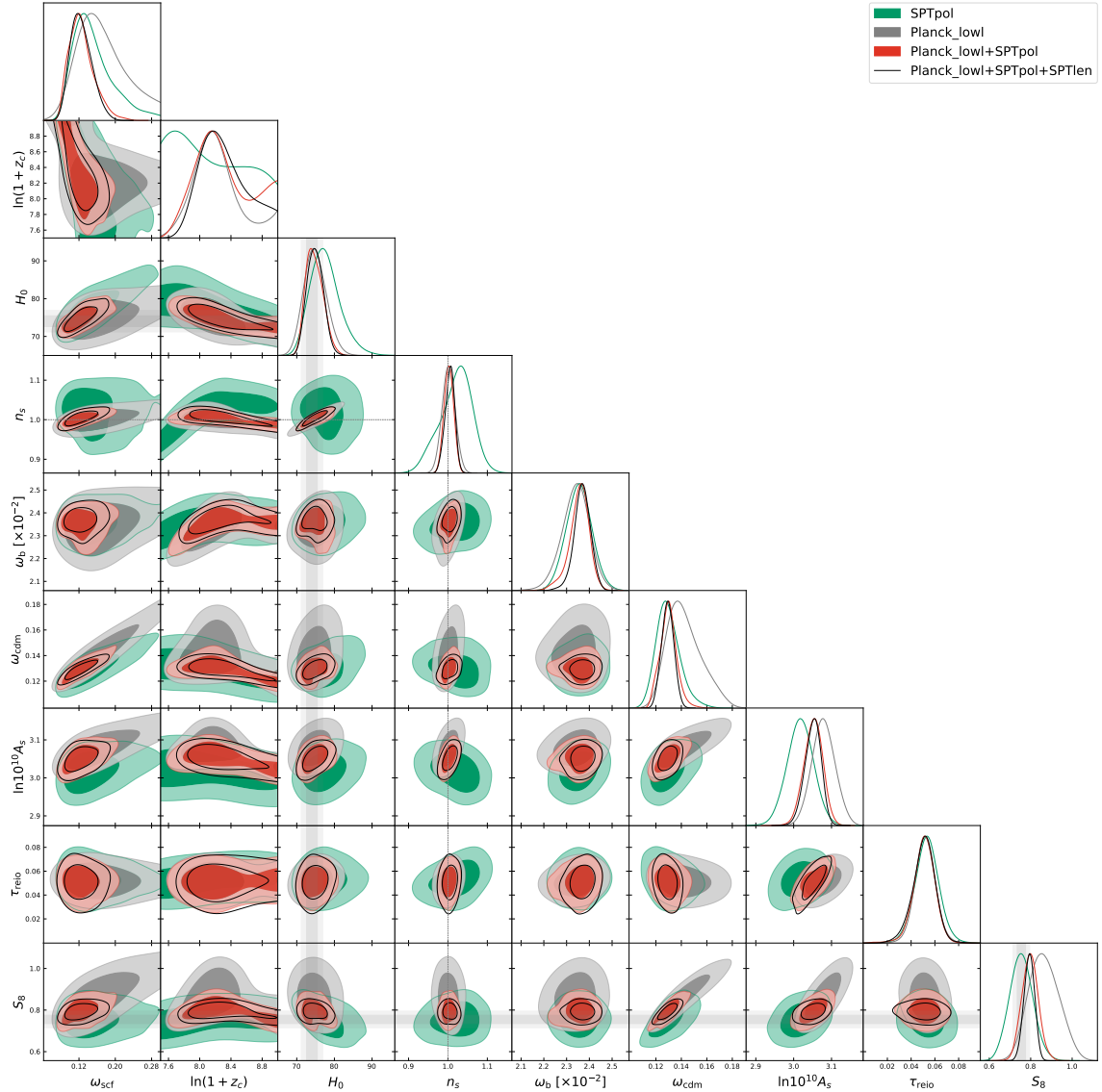


Figure 2. Posterior distributions of CMB data sets (68% and 95% confidence range). We also plot the SH0ES constraint to H_0 [5] and the KiDS+VIKING-450+DES-Y1 constraint to S_8 [78] in light gray.

recheck each part of CMB datasets under AdS-EDE model. We show the corresponding posterior distributions in Figure 2.

We see that they are still compatible under AdS-EDE due to large uncertainties in individual data sets. The differences between the cosmological parameters (including S_8) and AdS-EDE parameters are within 1σ between SPTpol and Planck_low ℓ . The region of the posterior distribution is reduced by the inclusion of SPTlen, but does not change significantly. This indicates that there is no significant conflict within the CMB data combination Planck_low ℓ +SPTpol+SPTlen.

parameters	Planck_low ℓ +SPT	Planck_low ℓ +SPT +BAO+Pantheon	Planck_low ℓ +SPT +BAO+Pantheon +SH0ES	Planck_low ℓ +SPT +BAO+Pantheon +SH0ES+RSD+WL
ω_{scf}	0.125(0.119) $^{+0.020}_{-0.027}$	0.111(0.099) $^{+0.010}_{-0.021}$	0.122(0.116) $^{+0.014}_{-0.021}$	0.1040(0.1016) $^{+0.0088}_{-0.014}$
$\ln(1+z_c)$	8.30(8.25) $^{+0.22}_{-0.37}$	8.52(8.47) \pm 0.24	8.39(8.30) $^{+0.17}_{-0.23}$	8.69(8.78) $^{+0.27}_{-0.12}$
H_0	74.9(74.7) \pm 2.1	72.24(71.92) $^{+0.86}_{-1.3}$	73.08(73.29) \pm 0.96	72.35(71.87) $^{+0.69}_{-0.90}$
n_s	1.005(1.007) $^{+0.013}_{-0.011}$	0.9908(0.9936) \pm 0.0092	0.9965(0.9990) $^{+0.0083}_{-0.0065}$	0.9893(0.9875) $^{+0.0076}_{-0.0087}$
ω_b	0.02369(0.02392) \pm 0.00036	0.02358(0.02386) \pm 0.00028	0.02368(0.02375) $^{+0.00033}_{-0.00027}$	0.02368(0.02367) \pm 0.00026
ω_{cdm}	0.1292(0.1292) \pm 0.0048	0.1292(0.1285) $^{+0.0035}_{-0.0046}$	0.1316(0.1308) \pm 0.0041	0.1253(0.1246) $^{+0.0021}_{-0.0027}$
$\ln 10^{10} A_s$	3.051(3.059) $^{+0.023}_{-0.019}$	3.042(3.042) $^{+0.021}_{-0.018}$	3.045(3.046) $^{+0.021}_{-0.016}$	3.025(3.026) $^{+0.020}_{-0.015}$
τ	0.0507(0.0545) $^{+0.010}_{-0.0082}$	0.0480(0.0489) $^{+0.0094}_{-0.0073}$	0.0462(0.0470) $^{+0.011}_{-0.0072}$	0.0457(0.0456) $^{+0.010}_{-0.0074}$
$100\theta_s$	1.04013(1.04052) \pm 0.00083	1.03946(1.03991) \pm 0.00070	1.03955(1.03965) \pm 0.00073	1.03932(1.03890) \pm 0.00070
σ_8	0.829(0.834) $^{+0.023}_{-0.015}$	0.822(0.823) \pm 0.018	0.831(0.832) $^{+0.017}_{-0.013}$	0.803(0.801) $^{+0.010}_{-0.012}$
S_8	0.793(0.799) \pm 0.025	0.814(0.818) \pm 0.020	0.820(0.816) $^{+0.020}_{-0.017}$	0.784(0.785) \pm 0.013

Table 1. Constraints on parameters under AdS-EDE for each data set, including mean values and $\pm 1\sigma$ regions, with best-fit values in parentheses.

5 Results

5.1 Planck_low ℓ + SPT

The constraints of our combined Planck_low ℓ +SPT dataset on the parameters are shown in the thick black solid line in [Figure 2](#) and [Table 1](#). A distinct non-Gaussian distribution can be found in the $\ln(1+z_c)$ - ω_{scf} plane, which is because in the low z_c and low ω_{scf} region θ_i is so small that the field would not climb out of AdS well (we called it AdS bound). However, our best-fit point is not close to this region, so we do not need to worry it. H_0 and ω_{scf} are positively correlated, which is exactly what we expect, i.e. larger EDE fraction brings a larger H_0 . Meanwhile, ω_{scf} and S_8 are negatively correlated, since larger ω_{cdm} is required to balance the extra EDE, we'll discuss it in detail in [section 6](#). The negative correlation between z_c and H_0 is due to very little effect of the EDE peak on r_s when EDE is far away from the recombination time.

Unlike other EDE solutions (such as [\[49\]](#) for the same dataset), CMB data alone has strong preference of non-zero EDE, at least for our model and dataset combination.² The posterior distributions of H_0 and S_8 are all consistent with direct measurements at 1σ level. The best value of H_0 is even slightly larger than R19. However, the uncertainty of H_0 is very large.

5.2 Planck_low ℓ + SPT + BAO + Pantheon

BAO measured $H(z)r_s^{\text{drag}}$ (line of sight direction) and $D_M(z)/r_s^{\text{drag}}$ (perpendicular to the line of sight direction), or average angle, constrained to $D_V(z)/r_s^{\text{drag}}$ for the late Universe, and (uncalibrated) supernova luminosity distances constrain the shape of $D_L(z)$, and thus the shape of $H(z)$. Their combination sets the constraint for $H_0 r_s^{\text{drag}}$. Recent studies have already pointed out that the Hubble tension is actually relevant with the deviations of both H_0 and r_s , e.g. [\[79–81\]](#), so it is necessary to compare the compatibility of model with BAO+SN observations. We add the data of BAO+Pantheon in our Planck_low ℓ +SPT

²But note that this is actually a reflection of AdS bound. Therefore we use best-fit values as our main result and mean values as assistance.

dataset and present the posterior distribution of the parameters in Figure 3, see also Table 1.

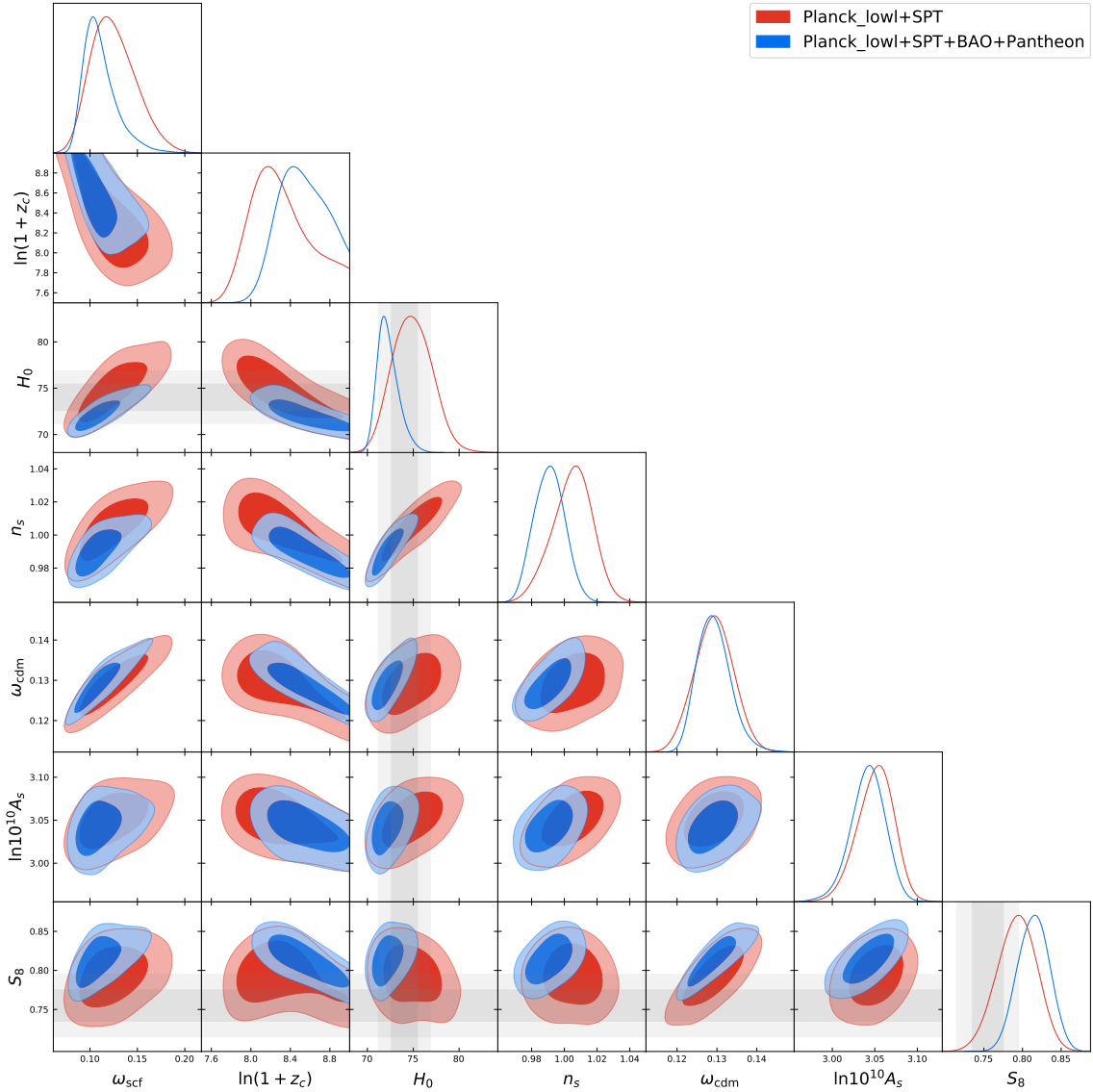


Figure 3. Planck_low ℓ +SPT (+BAO+Pantheon) constraints on each parameter under AdS-EDE (68% and 95% confidence range). We also plot the R19 constraint to H_0 [5] and the KiDS+VIKING-450+DES-Y1 constraint to S_8 [78] in light gray.

With the addition of BAO+Pantheon, the uncertainty of the parameters is much reduced, however the difference from the results without BAO+Pantheon stays within 1σ . This is an indication that BAO+Pantheon is compatible with our CMB dataset. $H_0 = 71.92$ is consistent with R19 at 1.1σ level, and is 3.7σ higher than that in Λ CDM model. The value of σ_8 is slightly raised, but is still 2.1σ consistent with the KiDS+VIKING-450+DES-Y1 (WL) result. The best-fit values of EDE fraction is slightly decreased after the addition of BAO+Pantheon.

We also compare the posterior distribution of the parameters in Figure 4 for our CMB dataset with those using the full Planck data (i.e., Planck2018 high- ℓ TT TE EE spectrum, low- ℓ TT EE spectrum and lensing spectrum) as CMB data, see also Table 5. The full Planck data has less parameter uncertainties, but its S_8 differs from the WL measurements by 4.9σ . H_0 in the full Planck data is slightly larger than that in our dataset, however, our EDE parameters, namely $\ln(1+z_c)$, ω_{scf} , have larger uncertainties.

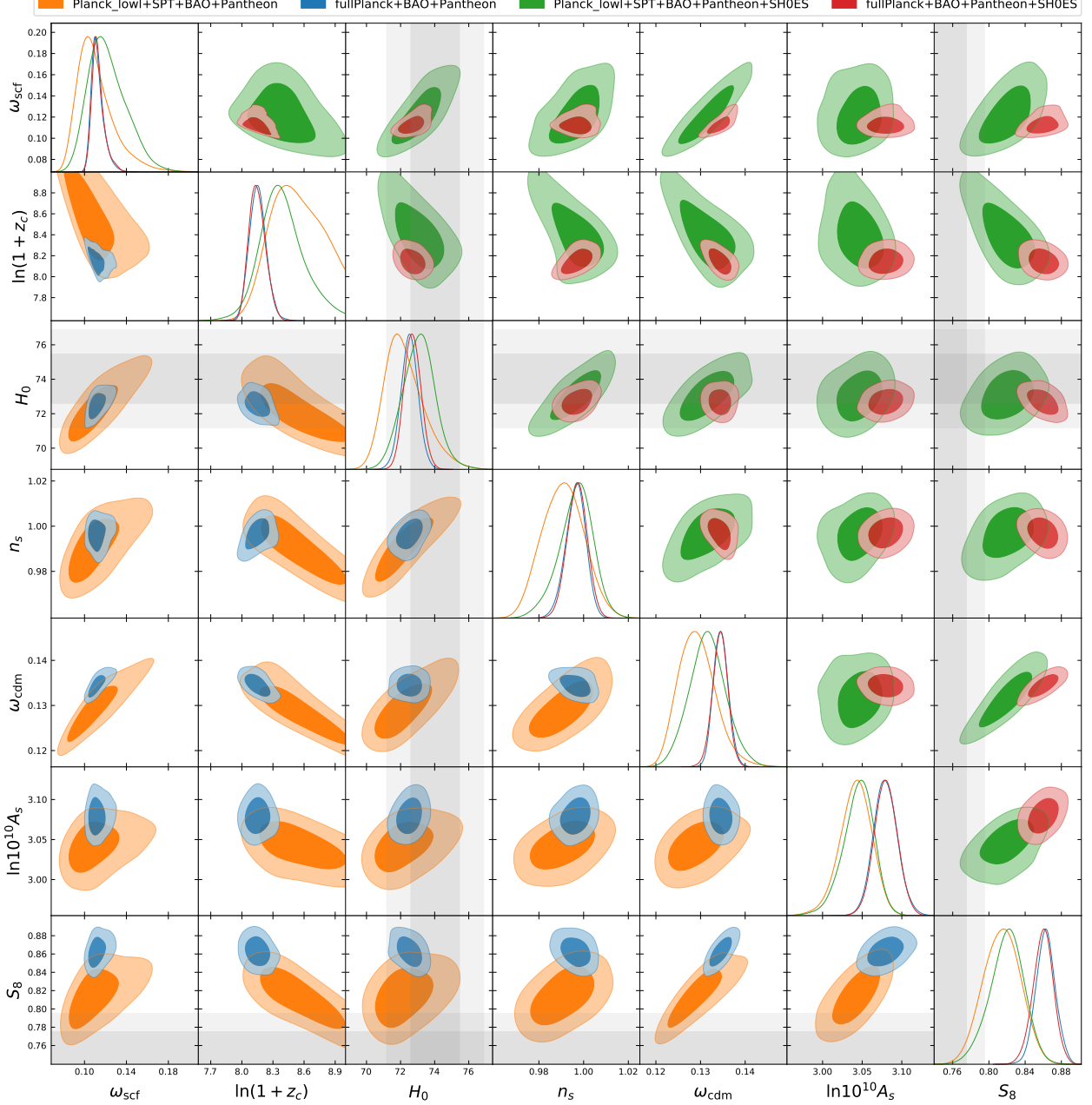


Figure 4. Constraints on each parameter for different combinations of CMB datasets + BAO + Pantheon (+SH0ES) under AdS-EDE (68% and 95% confidence range). We also plot the R19 constraint to H_0 [5] and the KiDS+VIKING-450+DES-Y1 constraint to S_8 [78] in light gray.

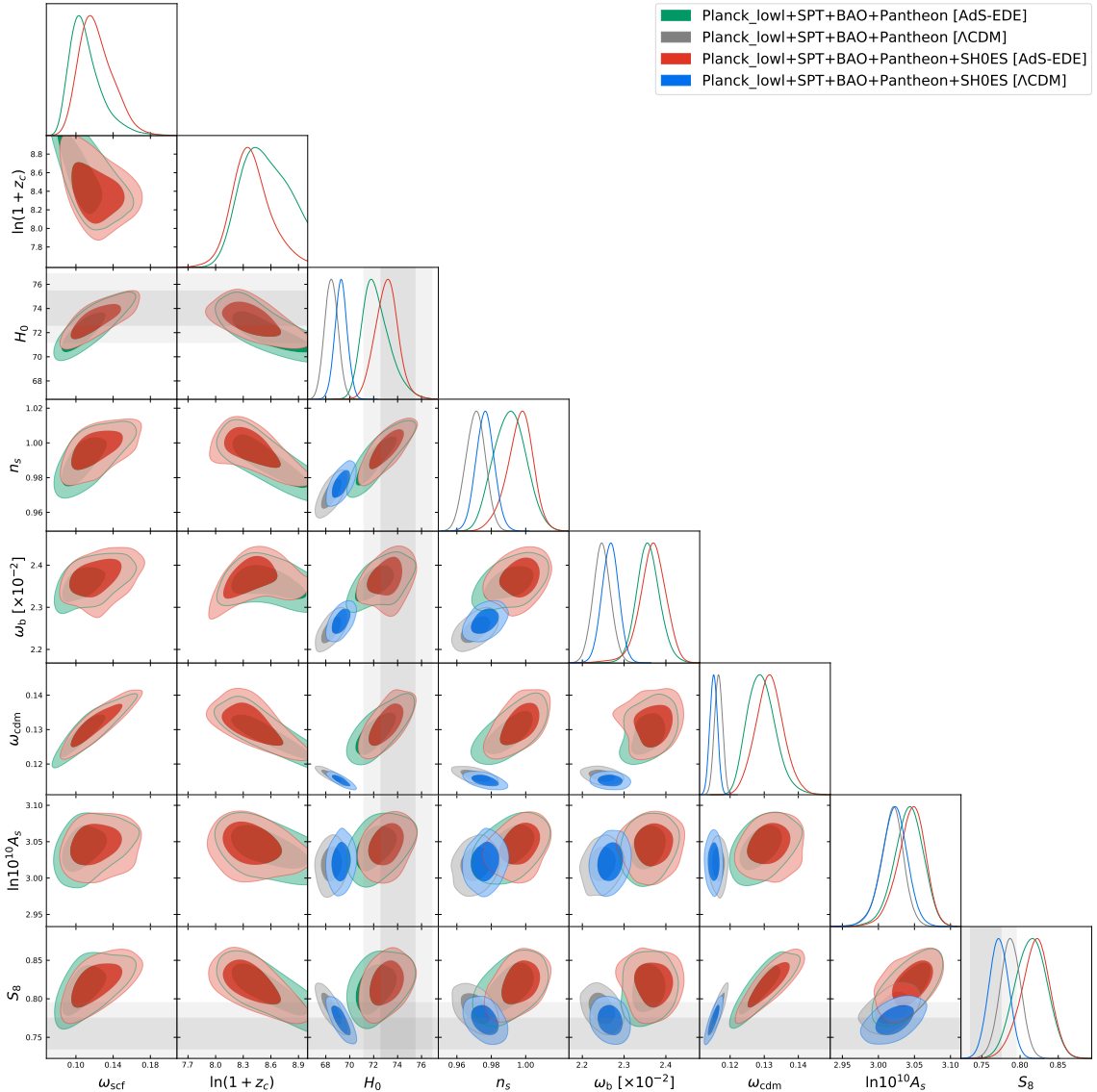


Figure 5. Constraints on the parameters by Planck_low ℓ +SPT+BAO+Pantheon (+SH0ES) under standard Λ CDM and AdS-EDE (68% and 95% confidence range). We also plot the R19 constraint to H_0 [5] and the KiDS+VIKING-450 + DES-Y1 constraint to S_8 [78] in light gray.

To further clarify the role of BAO+Pantheon, we follow [82][52] by approximating $H(z)$ as a five-point natural cubic spline function and fitting the BAO+Pantheon data with MCMC, constrain $\beta_{\text{BAO}} \equiv c / (H(z)r_s^{\text{drag}})$: $\beta_{\text{BAO}} = 29.769^{+0.379}_{-0.372}$. This constraint is model-independent (except for the flatness assumption). We compare the parameter constraints on the $r_s^{\text{drag}}-H_0$ plane under AdS-EDE with model-independent BAO+Pantheon in Figure 6.

It can be seen that the $r_s^{\text{drag}}-H_0$ distribution under AdS-EDE (without BAO+Pantheon data) is 1σ consistent with the overlap region of model-independent $r_s^{\text{drag}}-H_0$ constraint and R19. However, for Λ CDM (see e.g. [79]), its posterior distribution is far from the

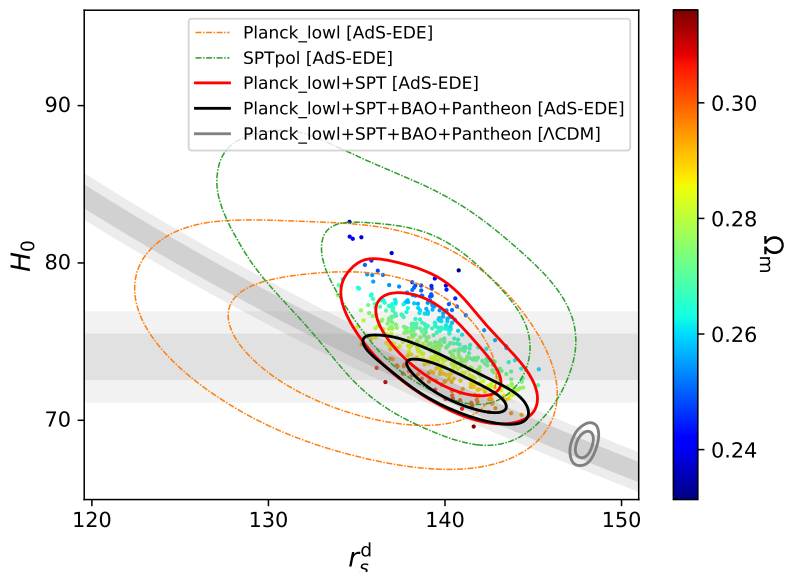


Figure 6. 1σ and 2σ posterior distributions for different model and dataset combinations in the $r_s^{\text{drag}}-H_0$ plane. The horizontal gray line is the R19 constraint on H_0 [5]. The skewed gray line is the BAO+Pantheon constraint on $H_0 r_s^{\text{drag}}$ in a model-independent way. The middle colored scatters are the parameters ranges in AdS-EDE constrained by Planck_low ℓ +SPT+BAO+Pantheon.

Data set	Λ CDM	AdS-EDE
Planck TT, $30 \leq \ell < 1000$	405.96	409.71
Planck TT, $\ell < 30$	22.35	20.38
Planck EE $\ell < 30$	395.68	395.92
SPTpol	145.56	144.92
SPTlen	4.91	4.97
BOSS DR12 BAO	3.55	3.60
BAO low- z	2.30	2.09
Pantheon	1026.91	1027.27
Total	2007.23	2008.86

Table 2. χ^2 of Λ CDM and AdS-EDE for the Planck_low ℓ +SPT+BAO+Pantheon best-fit values.

overlap region, and the degeneracy direction is orthogonal to the distribution of the model-independent constraint. Similar to Λ CDM, the direction of Ω_m in AdS-EDE is orthogonal to the model-independent $r_s^{\text{drag}}-H_0$ constrained degeneracy direction. This can be understood as following. It is well-known that CMB almost fixed θ_s , and

$$\theta_s = \frac{r_s}{D_A} = \frac{r_s}{\int \frac{dz}{H(z)}} = \frac{r_s H_0}{\int \frac{dz}{\sqrt{\Omega_m(1+z)^3 + (1-\Omega_m)}}}. \quad (5.1)$$

This suggests that Ω_m will be determined by $r_s H_0$. Therefore, the addition of BAO+Pantheon data constrains Ω_m to larger values, so S_8 .

Data set	Λ CDM	AdS-EDE
Planck TT, $30 \leq \ell < 1000$	407.06	407.97
Planck TT, $\ell < 30$	20.95	20.34
Planck EE $\ell < 30$	395.70	396.27
SPTpol	142.93	145.07
SPTlen	5.65	5.09
BOSS DR12 BAO	7.96	4.31
BAO low- z	4.39	2.89
Pantheon	1027.46	1027.04
SH0ES	8.96	0.27
Total	2021.07	2009.25

Table 3. χ^2 of Λ CDM and AdS-EDE best fits to Planck_low ℓ +SPT+BAO+Pantheon+SH0ES.

We present in [Table 2](#) the χ^2 of the best fits of Λ CDM and AdS-EDE. The AdS-EDE fit is slightly worse than the fit in Λ CDM: $\Delta\chi^2 = 1.63$. However, since the difference in χ^2 is slight, it is not statistically significant.

5.3 Planck_low ℓ + SPT + BAO + Pantheon + SH0ES

Including the R19 prior, we present the posterior parameters in [Table 1](#). We also present a comparison of the parameter posterior distribution before and after the addition of R19 data and with Λ CDM model in [Figure 5](#), and a comparison with the parameter posterior distribution using the full Planck data as CMB data instead in [Figure 4](#).

We see that H_0 is restricted to a higher value of $H_0 = 73.29$ (consistent with R19 within 1σ), and $S_8 = 0.816$. However, the uncertainty of H_0 does not enlarge significantly, which indicates that there is no significant inconsistency with R19 data. Thanks to the larger uncertainty of H_0 toward higher values without R19 prior for Planck_low ℓ +SPT dataset, H_0 is raised more than that for full Planck data (see [Appendix B](#)). Here, ω_{scf} is slightly raised and z_c is constrained to be closer to the recombination epoch to lift H_0 . However, this constraint on the EDE parameters is not as drastic as other EDE models, since AdS-EDE already brings a larger H_0 even without the H_0 prior.

Similarly, we present the χ^2 of the Λ CDM and AdS-EDE best-fit values with R19 data in [Table 3](#). After the addition of R19 data, the fit of Λ CDM to the BAO and Pantheon is bad due to the previously described deviation in the $r_s^{\text{darg}}-H_0$ plane. However, AdS-EDE is fully compatible with the H_0 prior. And due to its reduced r_s , the fit to the BAO and Pantheon measurements is also well. Due to the rapid decay of AdS-EDE, the spoil to the CMB fit is slight. Totally, we get $\Delta\chi^2 = -11.82$ for AdS-EDE compared to Λ CDM, indicating that AdS-EDE significantly fits relevant observations better than Λ CDM.

5.4 Planck_low ℓ + SPT + BAO + Pantheon + SH0ES + RSD + WL

Finally, we add RSD and WL measurements to make the relationship with direct S_8 measurements clear. Results are presented in [Figure 7](#) and [Table 1](#).

Including RSD+WL, we get $S_8 = 0.785$, the difference with direct S_8 measurement is only 1.3σ , while we have $H_0 = 71.87$, which is only slightly lower compared to that without RSD+WL. Compared with the result of full Planck data, Planck_low ℓ +SPT allows higher z_c , so that less ω_{cdm} is added to balance EDE, allowing to achieve a lower S_8 . This is different from compromise of lowering EDE fraction when the full Planck data is considered. Our results indicate that AdS-EDE is not excluded by the current WL measurements. As a contrast, we also present the result using EFTofLSS in Appendix [Appendix A](#).

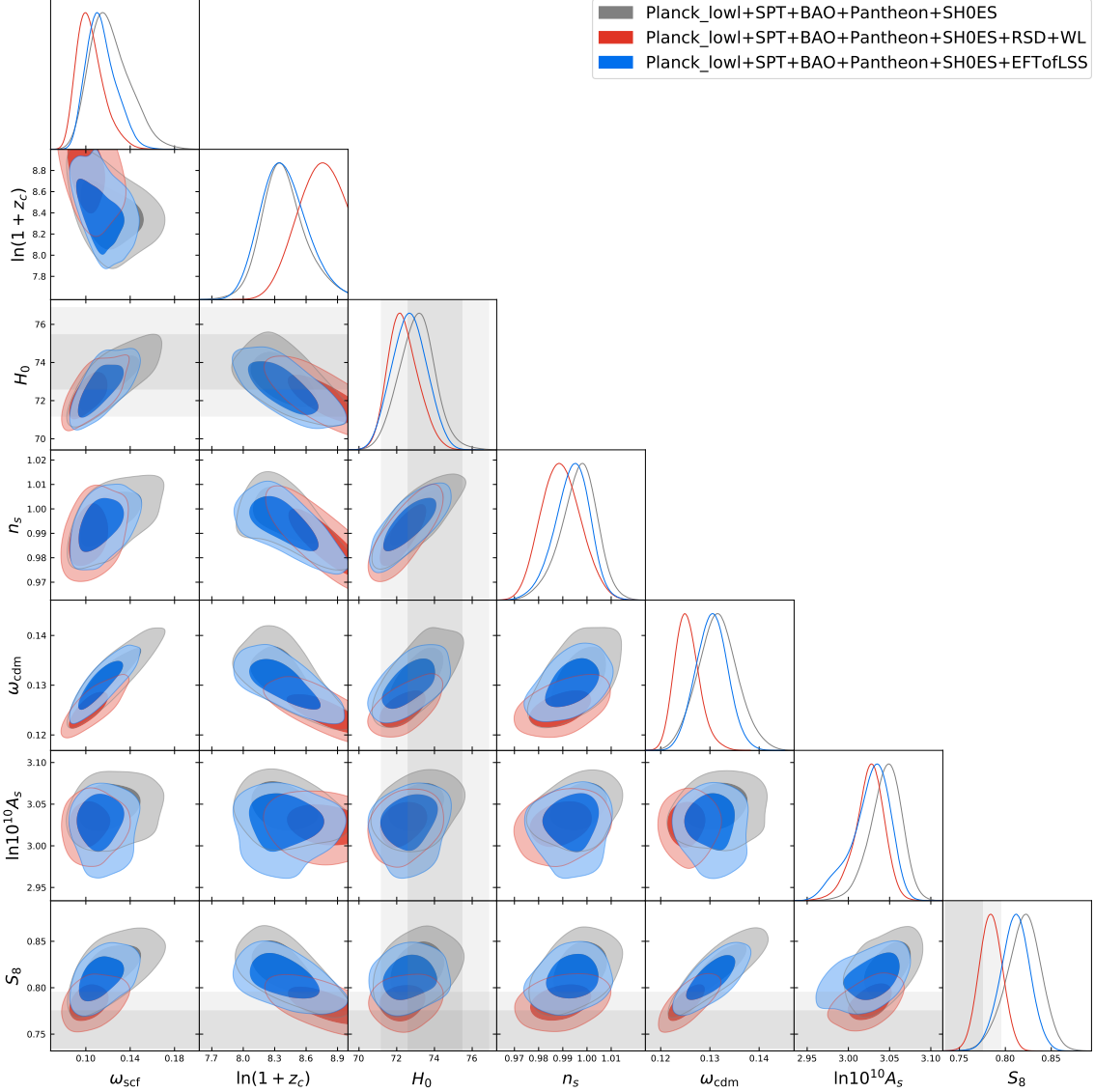


Figure 7. Posterior distribution of each parameter under AdS-EDE after adding RSD and WL measurements (68% and 95% confidence range). We also plot the R19 constraint to H_0 [5] and the KiDS+VIKING-450+DES-Y1 constraint to S_8 [78] in light gray.

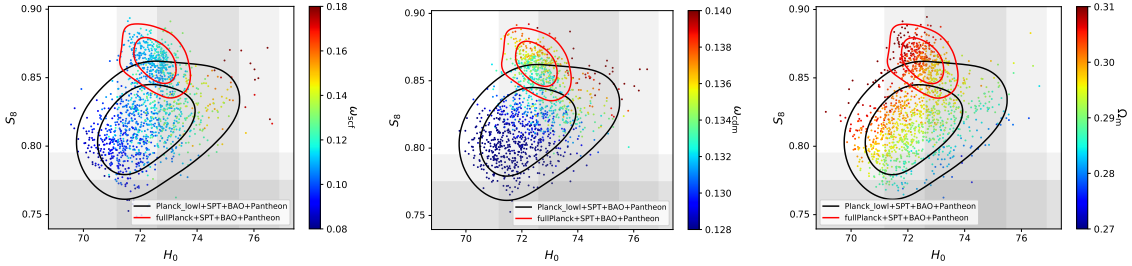


Figure 8. Parameters distribution on the plane (S_8, H_0) for Planck_lowl+SPT+BAO+Pantheon and fullPlanck+SPT+BAO+Pantheon in AdS-EDE. The gray bands represents constraints from direct H_0 [5] and S_8 [78] measurements.

6 Discussion

The S_8 - H_0 relation for our datasets is presented in Figure 8. We can find that EDE has a different relationship from Λ CDM (see e.g. Figure 5). Precise CMB θ_s^* measurement constrains $\omega_{\text{cdm}}H_0^{1.4}$ and the heights of peaks constrain ω_m , and they actually constrain $\omega_{\text{cdm}}H_0$ [3]. ω_{cdm} controls the late matter fluctuation, this is the reason of the negative relation in Figure 5.

However, this is not the case for EDE, since the relation of S_8 - H_0 is mainly controlled by EDE's fraction ω_{scf} , see left plane of Figure 8. In EDE scenario, since larger EDE fraction brings higher H_0 , larger ω_{cdm} required to balance early ISW effect (see middle panel of Figure 8), which is common in any early resolution (relevant with energy injection) for the Hubble tension. And the approximate relationship is $\frac{\delta H_0}{H_0} \simeq 0.5 \frac{\delta \omega_{\text{cdm}}}{\omega_{\text{cdm}}}$ [83]. It is this higher ω_{cdm} that bring larger S_8 .

Besides difference with Λ CDM, there is also difference between different CMB datasets, where Planck_lowl+SPT favors the region consistent with direct H_0 and S_8 measurements. This is relevant with $\Omega_m = \omega_m h^{-2}$ (see the right panel of Figure 8). As we have mentioned, BAO+SN data will precisely set Ω_m . However, this is the case only when θ_s is fixed. It can be found in Figure 9 that Planck_lowl+SPT favors a smaller θ_s , which will bring less Ω_m . It seems that the slightly less Ω_m than Planck has been indicated [84–88]. Here, the change of n_s is the natural results of higher H_0 [83].

To clarify the effect of different CMB datasets, we plot their best-fit values and residuals to Planck 2018 on TT and EE spectrum in Figure 10 and Figure 11. It can be found in Figure 11 that SPTpol polarization spectrum has smaller uncertainty than Planck at $\ell > 1000$ and can extend to higher ℓ . The different oscillation phases can be observed and the fullPlanck case is closer to the baseline model (as our baseline model contains fullPlanck data), which are indications for different θ_s . This different θ_s is due to the oscillation-like residuals in Planck's TT spectrum, which cause high-low ℓ inconsistency and lensing anomaly³. It also comes from oscillation-like residuals in Planck's TE and EE spectrum, which have not still detected in ACT or SPT observation [24].

³However, it is worth noting that our model also captures $800 < \ell < 1000$ residual peaks of Planck TT.

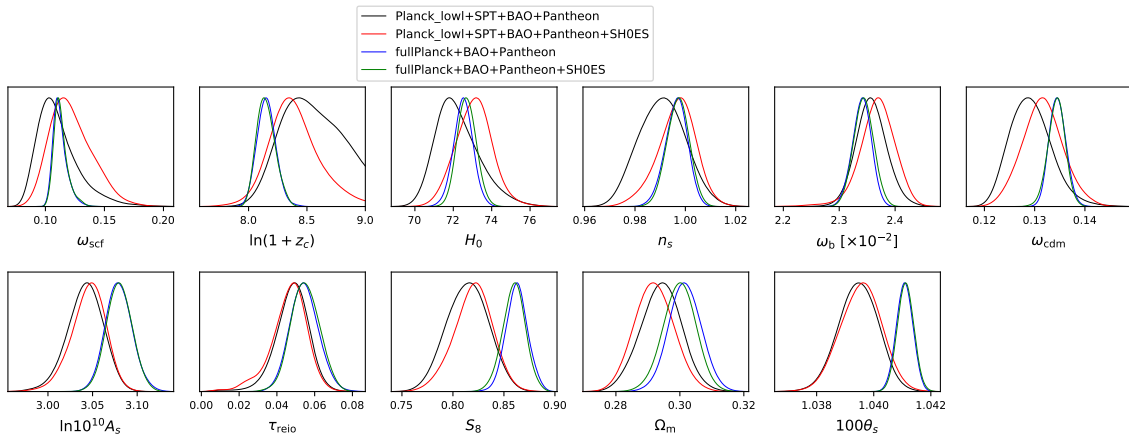


Figure 9. Posterior distribution of parameters in AdS-EDE using different CMB datasets.

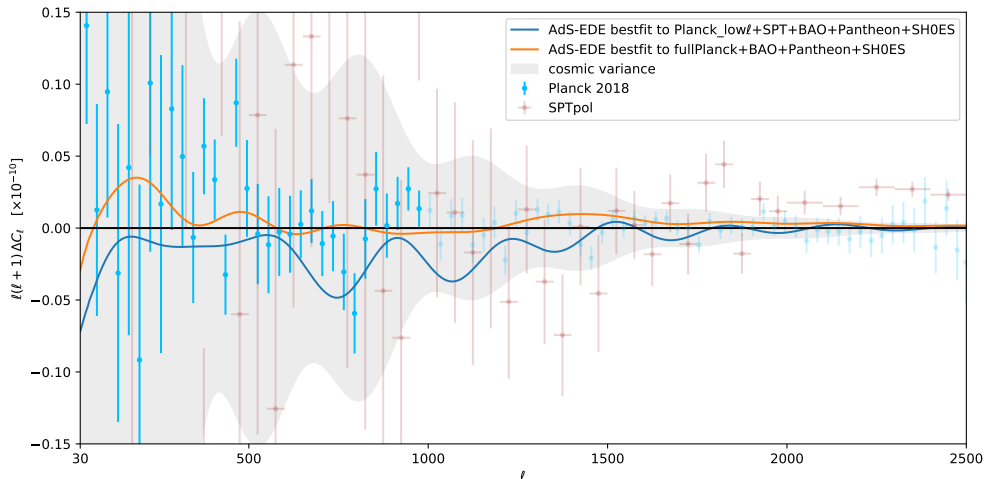


Figure 10. AdS-EDE best-fit values for Planck_low ℓ +SPT+BAO+Pantheon+SH0ES and fullPlanck+BAO+Pantheon+SH0ES on TT spectrum, and residual and uncertainty of different CMB observations (light error bars is the unused data). The reference value is the best-fit result to full Planck data (i.e. `base_plikHM_TTTEEE_lowl_lowE_lensing`) under Λ CDM model. Cosmological variance is showed in light gray background. Note different ℓ range to other figures.

Regardless of which CMB dataset is used, compared with the Λ CDM model larger n_s brings a deficit in the $\ell < 30$ multipoles. And this deficit does exist in Planck’s observations of the TT spectrum, which is one of the sources of its high and low ℓ inconsistency [44]. This leads to a better fit of AdS-EDE to this part of data, although not significant due to extremely large cosmological variance here.

We also compare the residuals of AdS-EDE with the cosmological variance, see Fig-

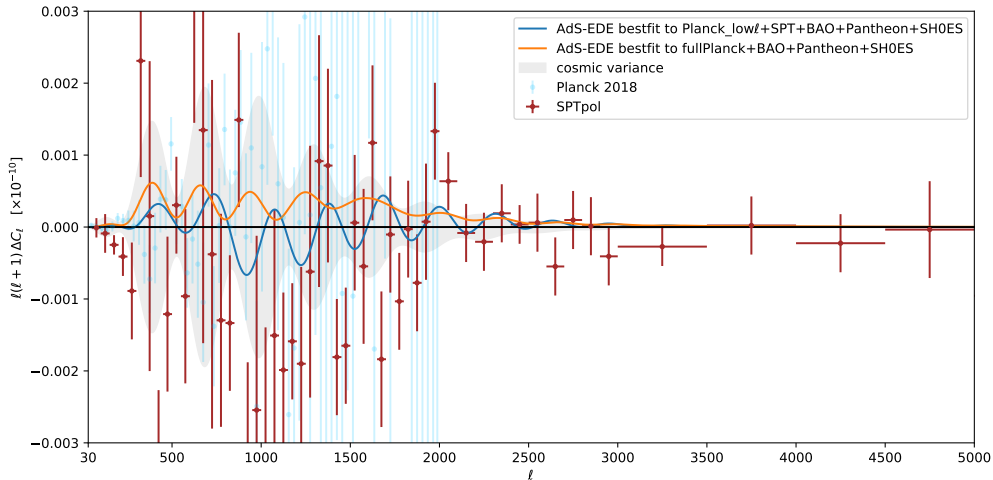


Figure 11. AdS-EDE best-fit values for Planck_low ℓ +SPT+BAO+Pantheon+SH0ES and fullPlanck+BAO+Pantheon+SH0ES on EE spectrum, and residual and uncertainty of different CMB observations (light error bars is the unused data). The reference value is the best-fit result to full Planck data (i.e. `base_plikHM_TTTEEE_lowl_lowE_lensing`) under Λ CDM model.

Figure 12. The residuals of the TT spectrum can only be within the cosmological variance for scales that can be observed at present ($\ell \leq 4000$), however, the residuals of the EE spectrum is larger than the cosmological variance at small scales ($2500 \lesssim \ell \leq 4000$). This suggests that the polarization spectrum will be a significant tool for constraining AdS-EDE from CMB, a range that also lies outside Planck’s multipoles. Due to the larger n_s , the AdS-EDE effect on very small scales also far exceeds the cosmological variance.

7 Conclusion

Currently, the EDE is a popular resolution for the Hubble tension. In AdS-EDE model, the existence of AdS phase can make the energy injected before recombination decay faster, which avoids degrading the CMB fit, and thus allow a higher EDE fraction. However, like other EDE models, this brings a larger late matter density fluctuation, worsening the tension between Planck data and LSS observations. Thus it is significant to revisit the constraining power of LSS on the AdS-EDE model using the different CMB dataset.

It is well-known that the Planck data itself also present the outstanding anomalies, such as the discrepancy between high and low ℓ and the over-smoothing of the acoustic peak by the gravitational lensing. Thus for CMB data, we conservatively discard the high ℓ part of Planck TT spectrum as well as the polarization spectrum and replace the corresponding data with SPTpol observations, as in Refs.[48, 49]. We verify the compatibility of this combined CMB dataset under AdS-EDE.

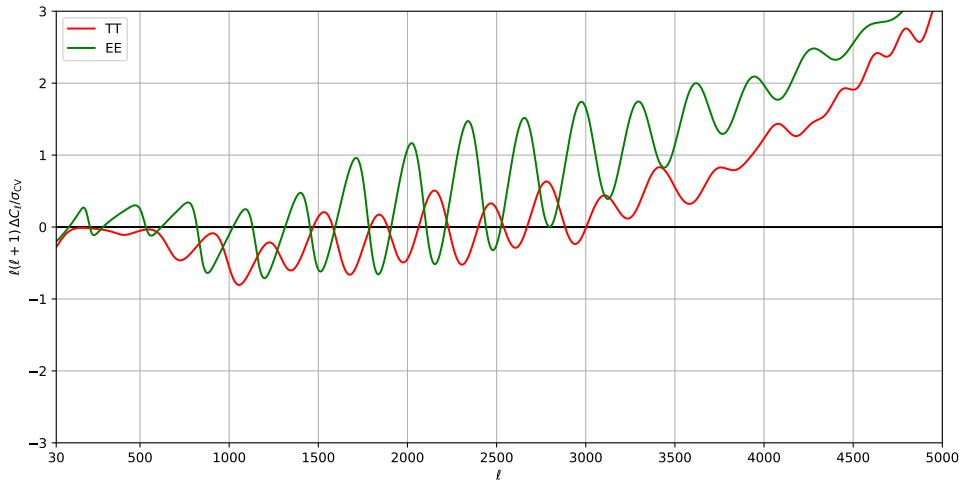


Figure 12. The AdS-EDE best-fit values for Planck_low ℓ +SPT+BAO+Pantheon+SH0ES compared with the best-fit values for the Λ CDM model based only on full Planck data (i.e., `base_plikHM_TTTEEE_lowl_lowE_lensing`) in term of the ratio of residuals to cosmological variance on the CMB TT and EE spectra.

We get $H_0 = 74.7$ km/s/Mpc when using our combined CMB dataset alone (Planck_low ℓ +SPT), and $H_0 = 71.92$ km/s/Mpc when using Planck_low ℓ +SPT+BAO+Pantheon dataset, respectively. Here, the Hubble tension is substantially relieved, even without any prior of direct measurements.⁴ And it is consistent with the age constraints of the oldest astrophysical objects [89] (see also [90–93] for other age constraints). Unlike other works (e.g. [37, 49]), we can see a preference for the non-zero AdS-EDE, with the best-fit value $\omega_{\text{scf}} \approx 0.1$. This is actually a straight result of the AdS bound in AdS-EDE model, which is not present without the AdS phase.

We also investigated the role of different CMB datasets. We find that the direction of solving both H_0 tension and S_8 tension is controlled by Ω_m , which is related to θ_s . The oscillation-like residual at high- ℓ part of Planck data, which is relative to lensing anomaly and high-low ℓ inconsistency, results in the corresponding discrepancy of θ_s . The residual analysis shows that the small-scale polarization spectrum is essential for identifying EDE models. Ground-based CMB experiments such as SPT-3G [94] and Advanced ACTPol [95] might observe effects of EDE on the CMB, while the upcoming high-precision small-scale CMB experiments Simons Observatory [96] and CMB-S4 [97] can help us to reestimate the anomaly at Planck’s high- ℓ part.

It should be also pointed out that the observations of LSS such as Euclid satellite [98], LSST [99], DESI [100] will not only further constraint on the resolution of the H_0 tension,

⁴With the H_0 prior from SH0ES, we get $H_0 = 73.29$ km/s/Mpc. Inclusion of the RSD and WL measurements leads to $S_8 = 0.785$, which is 1.3σ consistent with direct S_8 measurement.

but also enable us to judge whether the S_8 tension actually implies new physics or not.

Acknowledgments

We thank Gen Ye for helpful discussions. This work is supported by NSFC, Nos.12075246, 11690021, and also UCAS Undergraduate Innovative Practice Project.

A Results with Planck_low ℓ + SPT + BAO + Pantheon + SH0ES + EFTofLSS

Effective Field Theory of Large-Scale Structure (EFTofLSS) [101, 102] can extract information on moderate nonlinear scales, by characterizing the nonlinear effects on small scales as effective parameters on large scales. Since LSS is 3-dimensional, it will have larger number of modes than the 2-dimensional CMB, and thus can have a smaller cosmological variance and theoretically better constrain cosmological parameters.

Here, our BOSS DR12 BAO data are replaced with the data of BOSS DR12 containing three regions [103]: CMASS NGC, CMASS SGC and LOWZ NGC, as well as the covariance matrix between them. In principle, this statistical constraint on BAO data selection is worse than the ‘consensus’ final result used in our text. We consider the similar model-independent approach to obtain this BAO+Pantheon constraint on $r_s^{\text{drag}} H_0$: $\beta_{\text{BAO}} = 29.684^{+0.390}_{-0.386}$. There is no significant difference from the analysis result in the text, which indicates that it is safe to use this BAO alternative. The EFTofLSS is implemented by pybird [104]. The nuisance parameter of EFTofLSS is partially marginalized, and the rest are the same as [104], independent on echo area.

A comparison of the posterior distribution of the parameters before and after including EFTofLSS is presented in Figure 7 and Table 4. It can be seen that the degradation of the parameters is smaller than RSD+WL. Including EFTofLSS, we have $H_0 = 72.34$ km/s/Mpc, the discrepancy with R19 is only 0.8σ , the S_8 is only reduced by less than 1σ , and the uncertainty does not increase significantly.

parameters	Planck_low ℓ +SPT+BAO+Pantheon+SH0ES	Planck_low ℓ +SPT+BAO+Pantheon+SH0ES+EFTofLSS
ω_{scf}	$0.122(0.116)^{+0.014}_{-0.021}$	$0.114(0.108)^{+0.010}_{-0.016}$
$\ln(1+z_c)$	$8.39(8.30)^{+0.17}_{-0.23}$	$8.39(8.50)^{+0.19}_{-0.24}$
H_0	$73.08(73.29) \pm 0.96$	$72.68(72.34) \pm 0.91$
n_s	$0.9965(0.9990)^{+0.0083}_{-0.0065}$	$0.9938(0.9945)^{+0.0079}_{-0.0063}$
ω_b	$0.02368(0.02375)^{+0.00033}_{-0.00027}$	$0.02355(0.02373)^{+0.00029}_{-0.00025}$
ω_{cdm}	$0.1316(0.1308) \pm 0.0041$	$0.1304(0.1292) \pm 0.0032$
$\ln 10^{10} A_s$	$3.045(3.046)^{+0.021}_{-0.016}$	$3.027(3.030)^{+0.028}_{-0.016}$
τ	$0.0462(0.0470)^{+0.011}_{-0.0072}$	$0.0382(0.0434)^{+0.015}_{-0.0077}$
$100\theta_s$	$1.03955(1.03965) \pm 0.00073$	$1.03963(1.04010) \pm 0.00070$
σ_8	$0.831(0.832)^{+0.017}_{-0.013}$	$0.821(0.819)^{+0.015}_{-0.013}$
S_8	$0.820(0.816)^{+0.020}_{-0.017}$	$0.811(0.810) \pm 0.016$

Table 4. Constraints on the parameters of AdS-EDE for Planck_low ℓ + SPT + BAO + Pantheon + SH0ES (+ EFTofLSS), including mean values and $\pm 1\sigma$ regions, with best-fit values in parentheses.

B Results with fullPlanck+BAO+Pantheon

parameters	fullPlanck+BAO+Pantheon
ω_{scf}	$0.1124(0.1084)^{+0.0038}_{-0.0070}$
$\ln(1 + z_c)$	$8.153(8.147)^{+0.075}_{-0.084}$
H_0	$72.52(72.46) \pm 0.51$
n_s	$0.9964(0.9949)^{+0.0047}_{-0.0041}$
ω_b	$0.02341(0.02331)^{+0.00018}_{-0.00016}$
ω_{cdm}	$0.1346(0.1336)^{+0.0016}_{-0.0018}$
$\ln 10^{10} A_s$	$3.079(3.072) \pm 0.015$
τ	$0.0545(0.0523)^{+0.0071}_{-0.0079}$
$100\theta_s$	$1.04108(1.04132) \pm 0.00029$
σ_8	$0.8604(0.8554) \pm 0.0074$
S_8	$0.863(0.856) \pm 0.011$

Table 5. Constraints on the parameters of AdS-EDE for fullPlanck+BAO+Pantheon, including mean values and $\pm 1\sigma$ regions, with best-fit values in parentheses.

References

- [1] L. Verde, T. Treu, and A. G. Riess, *Tensions between the Early and the Late Universe*, *Nature Astron.* **3** (7, 2019) 891, [[arXiv:1907.10625](#)].
- [2] A. G. Riess, *The Expansion of the Universe is Faster than Expected*, *Nature Rev. Phys.* **2** (2019), no. 1 10–12, [[arXiv:2001.03624](#)].
- [3] **Planck** Collaboration, N. Aghanim et al., *Planck 2018 results. VI. Cosmological parameters*, *Astron. Astrophys.* **641** (2020) A6, [[arXiv:1807.06209](#)]. [Erratum: *Astron. Astrophys.* 652, C4 (2021)].
- [4] **eBOSS** Collaboration, S. Alam et al., *Completed SDSS-IV extended Baryon Oscillation Spectroscopic Survey: Cosmological implications from two decades of spectroscopic surveys at the Apache Point Observatory*, *Phys. Rev. D* **103** (2021), no. 8 083533, [[arXiv:2007.08991](#)].
- [5] A. G. Riess, S. Casertano, W. Yuan, L. M. Macri, and D. Scolnic, *Large Magellanic Cloud Cepheid Standards Provide a 1% Foundation for the Determination of the Hubble Constant and Stronger Evidence for Physics beyond Λ CDM*, *Astrophys. J.* **876** (2019), no. 1 85, [[arXiv:1903.07603](#)].
- [6] E. Di Valentino et al., *Snowmass2021 - Letter of interest cosmology intertwined II: The hubble constant tension*, *Astropart. Phys.* **131** (2021) 102605, [[arXiv:2008.11284](#)].
- [7] E. Di Valentino, O. Mena, S. Pan, L. Visinelli, W. Yang, A. Melchiorri, D. F. Mota, A. G. Riess, and J. Silk, *In the realm of the Hubble tension—a review of solutions*, *Class. Quant. Grav.* **38** (2021), no. 15 153001, [[arXiv:2103.01183](#)].
- [8] L. Perivolaropoulos and F. Skara, *Challenges for Λ CDM: An update*, [[arXiv:2105.05208](#)].
- [9] C. Heymans et al., *KiDS-1000 Cosmology: Multi-probe weak gravitational lensing and spectroscopic galaxy clustering constraints*, *Astron. Astrophys.* **646** (2021) A140, [[arXiv:2007.15632](#)].

- [10] H. Hildebrandt et al., *KiDS+VIKING-450: Cosmic shear tomography with optical and infrared data*, *Astron. Astrophys.* **633** (2020) A69, [[arXiv:1812.06076](#)].
- [11] R. C. Nunes and S. Vagnozzi, *Arbitrating the S8 discrepancy with growth rate measurements from redshift-space distortions*, *Mon. Not. Roy. Astron. Soc.* **505** (2021), no. 4 5427, [[arXiv:2106.01208](#)].
- [12] T. Karwal and M. Kamionkowski, *Dark energy at early times, the Hubble parameter, and the string axiverse*, *Phys. Rev. D* **94** (2016), no. 10 103523, [[arXiv:1608.01309](#)].
- [13] V. Poulin, T. L. Smith, T. Karwal, and M. Kamionkowski, *Early Dark Energy Can Resolve The Hubble Tension*, *Phys. Rev. Lett.* **122** (2019), no. 22 221301, [[arXiv:1811.04083](#)].
- [14] T. L. Smith, V. Poulin, and M. A. Amin, *Oscillating scalar fields and the Hubble tension: a resolution with novel signatures*, *Phys. Rev. D* **101** (2020), no. 6 063523, [[arXiv:1908.06995](#)].
- [15] P. Agrawal, F.-Y. Cyr-Racine, D. Pinner, and L. Randall, *Rock 'n' Roll Solutions to the Hubble Tension*, [[arXiv:1904.01016](#)].
- [16] M.-X. Lin, G. Benevento, W. Hu, and M. Raveri, *Acoustic Dark Energy: Potential Conversion of the Hubble Tension*, *Phys. Rev. D* **100** (2019), no. 6 063542, [[arXiv:1905.12618](#)].
- [17] F. Niedermann and M. S. Sloth, *New early dark energy*, *Phys. Rev. D* **103** (2021), no. 4 L041303, [[arXiv:1910.10739](#)].
- [18] T. Karwal, M. Raveri, B. Jain, J. Khoury, and M. Trodden, *Chameleon Early Dark Energy and the Hubble Tension*, [[arXiv:2106.13290](#)].
- [19] G. Ye and Y.-S. Piao, *Is the Hubble tension a hint of AdS phase around recombination?*, *Phys. Rev. D* **101** (2020), no. 8 083507, [[arXiv:2001.02451](#)].
- [20] G. Ye and Y.-S. Piao, *T_0 censorship of early dark energy and AdS vacua*, *Phys. Rev. D* **102** (2020), no. 8 083523, [[arXiv:2008.10832](#)].
- [21] S. Alexander and E. McDonough, *Axion-Dilaton Destabilization and the Hubble Tension*, *Phys. Lett. B* **797** (2019) 134830, [[arXiv:1904.08912](#)].
- [22] J. Sakstein and M. Trodden, *Early Dark Energy from Massive Neutrinos as a Natural Resolution of the Hubble Tension*, *Phys. Rev. Lett.* **124** (2020), no. 16 161301, [[arXiv:1911.11760](#)].
- [23] M. Braglia, W. T. Emond, F. Finelli, A. E. Gumrukcuoglu, and K. Koyama, *Unified framework for early dark energy from α -attractors*, *Phys. Rev. D* **102** (2020), no. 8 083513, [[arXiv:2005.14053](#)].
- [24] M.-X. Lin, W. Hu, and M. Raveri, *Testing H_0 in Acoustic Dark Energy with Planck and ACT Polarization*, *Phys. Rev. D* **102** (2020) 123523, [[arXiv:2009.08974](#)].
- [25] T. Fujita, K. Murai, H. Nakatsuka, and S. Tsujikawa, *Detection of isotropic cosmic birefringence and its implications for axionlike particles including dark energy*, *Phys. Rev. D* **103** (2021), no. 4 043509, [[arXiv:2011.11894](#)].
- [26] O. Seto and Y. Toda, *Comparing early dark energy and extra radiation solutions to the Hubble tension with BBN*, *Phys. Rev. D* **103** (2021), no. 12 123501, [[arXiv:2101.03740](#)].
- [27] S. X. Tian and Z.-H. Zhu, *Early dark energy in k-essence*, *Phys. Rev. D* **103** (2021), no. 4 043518, [[arXiv:2102.06399](#)].

- [28] V. I. Sabla and R. R. Caldwell, *No H_0 assistance from assisted quintessence*, *Phys. Rev. D* **103** (2021), no. 10 103506, [[arXiv:2103.04999](#)].
- [29] S. Nojiri, S. D. Odintsov, D. Saez-Chillon Gomez, and G. S. Sharov, *Modeling and testing the equation of state for (Early) dark energy*, *Phys. Dark Univ.* **32** (2021) 100837, [[arXiv:2103.05304](#)].
- [30] M. Braglia and S. Kuroyanagi, *Probing pre-Recombination Physics by the Cross-Correlation of Stochastic Gravitational Waves and CMB Anisotropies*, [arXiv:2106.03786](#).
- [31] I. J. Allali, M. P. Hertzberg, and F. Rompineve, *A Dark Sector to Restore Cosmological Concordance*, [arXiv:2104.12798](#).
- [32] M. Zumalacarregui, *Gravity in the Era of Equality: Towards solutions to the Hubble problem without fine-tuned initial conditions*, *Phys. Rev. D* **102** (2020), no. 2 023523, [[arXiv:2003.06396](#)].
- [33] G. Ballesteros, A. Notari, and F. Rompineve, *The H_0 tension: ΔG_N vs. ΔN_{eff}* , *JCAP* **11** (2020) 024, [[arXiv:2004.05049](#)].
- [34] M. Braglia, M. Ballardini, F. Finelli, and K. Koyama, *Early modified gravity in light of the H_0 tension and LSS data*, *Phys. Rev. D* **103** (2021), no. 4 043528, [[arXiv:2011.12934](#)].
- [35] S. D. Odintsov, D. Sáez-Chillón Gómez, and G. S. Sharov, *Analyzing the H_0 tension in $F(R)$ gravity models*, *Nucl. Phys. B* **966** (2021) 115377, [[arXiv:2011.03957](#)].
- [36] M. G. Dainotti, B. De Simone, T. Schiavone, G. Montani, E. Rinaldi, and G. Lambiase, *On the Hubble constant tension in the SNe Ia Pantheon sample*, *Astrophys. J.* **912** (2021), no. 2 150, [[arXiv:2103.02117](#)].
- [37] J. C. Hill, E. McDonough, M. W. Toomey, and S. Alexander, *Early dark energy does not restore cosmological concordance*, *Phys. Rev. D* **102** (2020), no. 4 043507, [[arXiv:2003.07355](#)].
- [38] M. M. Ivanov, E. McDonough, J. C. Hill, M. Simonović, M. W. Toomey, S. Alexander, and M. Zaldarriaga, *Constraining Early Dark Energy with Large-Scale Structure*, *Phys. Rev. D* **102** (2020), no. 10 103502, [[arXiv:2006.11235](#)].
- [39] G. D’Amico, L. Senatore, P. Zhang, and H. Zheng, *The Hubble Tension in Light of the Full-Shape Analysis of Large-Scale Structure Data*, *JCAP* **05** (2021) 072, [[arXiv:2006.12420](#)].
- [40] S. Vagnozzi, *Consistency tests of Λ CDM from the early integrated Sachs-Wolfe effect: Implications for early-time new physics and the Hubble tension*, *Phys. Rev. D* **104** (2021), no. 6 063524, [[arXiv:2105.10425](#)].
- [41] R. Murgia, G. F. Abellán, and V. Poulin, *Early dark energy resolution to the Hubble tension in light of weak lensing surveys and lensing anomalies*, *Phys. Rev. D* **103** (2021), no. 6 063502, [[arXiv:2009.10733](#)].
- [42] T. L. Smith, V. Poulin, J. L. Bernal, K. K. Boddy, M. Kamionkowski, and R. Murgia, *Early dark energy is not excluded by current large-scale structure data*, *Phys. Rev. D* **103** (2021), no. 12 123542, [[arXiv:2009.10740](#)].
- [43] G. E. Addison, Y. Huang, D. J. Watts, C. L. Bennett, M. Halpern, G. Hinshaw, and J. L. Weiland, *Quantifying discordance in the 2015 Planck CMB spectrum*, *Astrophys. J.* **818** (2016), no. 2 132, [[arXiv:1511.00055](#)].

- [44] **Planck** Collaboration, N. Aghanim et al., *Planck intermediate results. LI. Features in the cosmic microwave background temperature power spectrum and shifts in cosmological parameters*, *Astron. Astrophys.* **607** (2017) A95, [[arXiv:1608.02487](#)].
- [45] P. Motloch and W. Hu, *Lensinglike tensions in the Planck legacy release*, *Phys. Rev. D* **101** (2020), no. 8 083515, [[arXiv:1912.06601](#)].
- [46] **ACT** Collaboration, S. Aiola et al., *The Atacama Cosmology Telescope: DR4 Maps and Cosmological Parameters*, *JCAP* **12** (2020) 047, [[arXiv:2007.07288](#)].
- [47] **SPT** Collaboration, J. W. Henning et al., *Measurements of the Temperature and E-Mode Polarization of the CMB from 500 Square Degrees of SPTpol Data*, *Astrophys. J.* **852** (2018), no. 2 97, [[arXiv:1707.09353](#)].
- [48] A. Chudaykin, D. Gorbunov, and N. Nedelko, *Combined analysis of Planck and SPTPol data favors the early dark energy models*, *JCAP* **08** (2020) 013, [[arXiv:2004.13046](#)].
- [49] A. Chudaykin, D. Gorbunov, and N. Nedelko, *Exploring an early dark energy solution to the Hubble tension with Planck and SPTPol data*, *Phys. Rev. D* **103** (2021), no. 4 043529, [[arXiv:2011.04682](#)].
- [50] J. C. Hill et al., *The Atacama Cosmology Telescope: Constraints on Pre-Recombination Early Dark Energy*, [arXiv:2109.04451](#).
- [51] V. Poulin, T. L. Smith, and A. Bartlett, *Dark Energy at early times and ACT: a larger Hubble constant without late-time priors*, [arXiv:2109.06229](#).
- [52] K. Aylor, M. Joy, L. Knox, M. Millea, S. Raghunathan, and W. L. K. Wu, *Sounds Discordant: Classical Distance Ladder & Λ CDM -based Determinations of the Cosmological Sound Horizon*, *Astrophys. J.* **874** (2019), no. 1 4, [[arXiv:1811.00537](#)].
- [53] R. Bousso and J. Polchinski, *Quantization of four form fluxes and dynamical neutralization of the cosmological constant*, *JHEP* **06** (2000) 006, [[hep-th/0004134](#)].
- [54] U. H. Danielsson, S. S. Haque, G. Shiu, and T. Van Riet, *Towards Classical de Sitter Solutions in String Theory*, *JHEP* **09** (2009) 114, [[arXiv:0907.2041](#)].
- [55] J. M. Maldacena, *The Large N limit of superconformal field theories and supergravity*, *Adv. Theor. Math. Phys.* **2** (1998) 231–252, [[hep-th/9711200](#)].
- [56] H. Ooguri and C. Vafa, *On the Geometry of the String Landscape and the Swampland*, *Nucl. Phys. B* **766** (2007) 21–33, [[hep-th/0605264](#)].
- [57] G. Obied, H. Ooguri, L. Spodyneiko, and C. Vafa, *De Sitter Space and the Swampland*, [arXiv:1806.08362](#).
- [58] S. K. Garg and C. Krishnan, *Bounds on Slow Roll and the de Sitter Swampland*, *JHEP* **11** (2019) 075, [[arXiv:1807.05193](#)].
- [59] Y.-S. Piao, *Can the universe experience many cycles with different vacua?*, *Phys. Rev. D* **70** (2004) 101302, [[hep-th/0407258](#)].
- [60] Y. Cai, Y. Wan, H.-G. Li, T. Qiu, and Y.-S. Piao, *The Effective Field Theory of nonsingular cosmology*, *JHEP* **01** (2017) 090, [[arXiv:1610.03400](#)].
- [61] H.-H. Li, G. Ye, Y. Cai, and Y.-S. Piao, *Trans-Planckian censorship of multistage inflation and dark energy*, *Phys. Rev. D* **101** (2020), no. 6 063527, [[arXiv:1911.06148](#)].

- [62] K. Dutta, Ruchika, A. Roy, A. A. Sen, and M. M. Sheikh-Jabbari, *Beyond Λ CDM with low and high redshift data: implications for dark energy*, *Gen. Rel. Grav.* **52** (2020), no. 2 15, [[arXiv:1808.06623](#)].
- [63] L. Visinelli, S. Vagnozzi, and U. Danielsson, *Revisiting a negative cosmological constant from low-redshift data*, *Symmetry* **11** (2019), no. 8 1035, [[arXiv:1907.07953](#)].
- [64] Ruchika, K. Dutta, A. Mukherjee, and A. A. Sen, *Observational Constraints on Axion(s) with a Cosmological Constant*, [[arXiv:2005.08813](#)].
- [65] R. Calderón, R. Gannouji, B. L’Huillier, and D. Polarski, *Negative cosmological constant in the dark sector?*, *Phys. Rev. D* **103** (2021), no. 2 023526, [[arXiv:2008.10237](#)].
- [66] D. Blas, J. Lesgourgues, and T. Tram, *The Cosmic Linear Anisotropy Solving System (CLASS) II: Approximation schemes*, *JCAP* **07** (2011) 034, [[arXiv:1104.2933](#)].
- [67] T. Brinckmann and J. Lesgourgues, *MontePython 3: boosted MCMC sampler and other features*, *Phys. Dark Univ.* **24** (2019) 100260, [[arXiv:1804.07261](#)].
- [68] B. Audren, J. Lesgourgues, K. Benabed, and S. Prunet, *Conservative Constraints on Early Cosmology: an illustration of the Monte Python cosmological parameter inference code*, *JCAP* **02** (2013) 001, [[arXiv:1210.7183](#)].
- [69] **VIRGO Consortium** Collaboration, R. E. Smith, J. A. Peacock, A. Jenkins, S. D. M. White, C. S. Frenk, F. R. Pearce, P. A. Thomas, G. Efstathiou, and H. M. P. Couchmann, *Stable clustering, the halo model and nonlinear cosmological power spectra*, *Mon. Not. Roy. Astron. Soc.* **341** (2003) 1311, [[astro-ph/0207664](#)].
- [70] R. Takahashi, M. Sato, T. Nishimichi, A. Taruya, and M. Oguri, *Revising the Halofit Model for the Nonlinear Matter Power Spectrum*, *Astrophys. J.* **761** (2012) 152, [[arXiv:1208.2701](#)].
- [71] A. Lewis, *GetDist: a Python package for analysing Monte Carlo samples*, [[arXiv:1910.13970](#)].
- [72] W. L. K. Wu et al., *A Measurement of the Cosmic Microwave Background Lensing Potential and Power Spectrum from 500 deg² of SPTpol Temperature and Polarization Data*, *Astrophys. J.* **884** (2019) 70, [[arXiv:1905.05777](#)].
- [73] **SPT** Collaboration, F. Bianchini et al., *Constraints on Cosmological Parameters from the 500 deg² SPTpol Lensing Power Spectrum*, *Astrophys. J.* **888** (2020) 119, [[arXiv:1910.07157](#)].
- [74] F. Beutler, C. Blake, M. Colless, D. H. Jones, L. Staveley-Smith, L. Campbell, Q. Parker, W. Saunders, and F. Watson, *The 6dF Galaxy Survey: Baryon Acoustic Oscillations and the Local Hubble Constant*, *Mon. Not. Roy. Astron. Soc.* **416** (2011) 3017–3032, [[arXiv:1106.3366](#)].
- [75] A. J. Ross, L. Samushia, C. Howlett, W. J. Percival, A. Burden, and M. Manera, *The clustering of the SDSS DR7 main Galaxy sample – I. A 4 per cent distance measure at $z = 0.15$* , *Mon. Not. Roy. Astron. Soc.* **449** (2015), no. 1 835–847, [[arXiv:1409.3242](#)].
- [76] **BOSS** Collaboration, S. Alam et al., *The clustering of galaxies in the completed SDSS-III Baryon Oscillation Spectroscopic Survey: cosmological analysis of the DR12 galaxy sample*, *Mon. Not. Roy. Astron. Soc.* **470** (2017), no. 3 2617–2652, [[arXiv:1607.03155](#)].
- [77] D. M. Scolnic et al., *The Complete Light-curve Sample of Spectroscopically Confirmed SNe*

- Ia from Pan-STARRS1 and Cosmological Constraints from the Combined Pantheon Sample*, *Astrophys. J.* **859** (2018), no. 2 101, [[arXiv:1710.00845](#)].
- [78] M. Asgari et al., *KiDS+VIKING-450 and DES-Y1 combined: Mitigating baryon feedback uncertainty with COSEBIs*, *Astron. Astrophys.* **634** (2020) A127, [[arXiv:1910.05336](#)].
- [79] L. Knox and M. Millea, *Hubble constant hunter’s guide*, *Phys. Rev. D* **101** (2020), no. 4 043533, [[arXiv:1908.03663](#)].
- [80] M.-Z. Lyu, B. S. Haridasu, M. Viel, and J.-Q. Xia, *H_0 Reconstruction with Type Ia Supernovae, Baryon Acoustic Oscillation and Gravitational Lensing Time-Delay*, *Astrophys. J.* **900** (2020), no. 2 160, [[arXiv:2001.08713](#)].
- [81] B. S. Haridasu, M. Viel, and N. Vittorio, *Sources of H_0 -tension in dark energy scenarios*, *Phys. Rev. D* **103** (2021), no. 6 063539, [[arXiv:2012.10324](#)].
- [82] J. L. Bernal, L. Verde, and A. G. Riess, *The trouble with H_0* , *JCAP* **10** (2016) 019, [[arXiv:1607.05617](#)].
- [83] G. Ye, B. Hu, and Y.-S. Piao, *Implication of the Hubble tension for the primordial Universe in light of recent cosmological data*, *Phys. Rev. D* **104** (2021), no. 6 063510, [[arXiv:2103.09729](#)].
- [84] M. Moresco, L. Pozzetti, A. Cimatti, R. Jimenez, C. Maraston, L. Verde, D. Thomas, A. Citro, R. Tojeiro, and D. Wilkinson, *A 6% measurement of the Hubble parameter at $z \sim 0.45$: direct evidence of the epoch of cosmic re-acceleration*, *JCAP* **05** (2016) 014, [[arXiv:1601.01701](#)].
- [85] S. Vagnozzi, E. Giusarma, O. Mena, K. Freese, M. Gerbino, S. Ho, and M. Lattanzi, *Unveiling ν secrets with cosmological data: neutrino masses and mass hierarchy*, *Phys. Rev. D* **96** (2017), no. 12 123503, [[arXiv:1701.08172](#)].
- [86] **DES** Collaboration, T. M. C. Abbott et al., *Dark Energy Survey year 1 results: Cosmological constraints from galaxy clustering and weak lensing*, *Phys. Rev. D* **98** (2018), no. 4 043526, [[arXiv:1708.01530](#)].
- [87] I. n. Zubeldia and A. Challinor, *Cosmological constraints from Planck galaxy clusters with CMB lensing mass bias calibration*, *Mon. Not. Roy. Astron. Soc.* **489** (2019), no. 1 401–419, [[arXiv:1904.07887](#)].
- [88] **KiDS** Collaboration, M. Asgari et al., *KiDS-1000 Cosmology: Cosmic shear constraints and comparison between two point statistics*, *Astron. Astrophys.* **645** (2021) A104, [[arXiv:2007.15633](#)].
- [89] S. Vagnozzi, F. Pacucci, and A. Loeb, *Implications for the Hubble tension from the ages of the oldest astrophysical objects*, [[arXiv:2105.10421](#)].
- [90] R. Jimenez, A. Cimatti, L. Verde, M. Moresco, and B. Wandelt, *The local and distant Universe: stellar ages and H_0* , *JCAP* **03** (2019) 043, [[arXiv:1902.07081](#)].
- [91] J. L. Bernal, L. Verde, R. Jimenez, M. Kamionkowski, D. Valcin, and B. D. Wandelt, *The trouble beyond H_0 and the new cosmic triangles*, *Phys. Rev. D* **103** (2021), no. 10 103533, [[arXiv:2102.05066](#)].
- [92] M. Boylan-Kolchin and D. R. Weisz, *Uncertain times: the redshift–time relation from cosmology and stars*, *Mon. Not. Roy. Astron. Soc.* **505** (2021), no. 2 2764–2783, [[arXiv:2103.15825](#)].

- [93] C. Krishnan, R. Mohayaee, E. O. Colgáin, M. M. Sheikh-Jabbari, and L. Yin, *Does Hubble tension signal a breakdown in FLRW cosmology?*, *Class. Quant. Grav.* **38** (2021), no. 18 184001, [[arXiv:2105.09790](#)].
- [94] **SPT-3G** Collaboration, B. A. Benson et al., *SPT-3G: A Next-Generation Cosmic Microwave Background Polarization Experiment on the South Pole Telescope*, *Proc. SPIE Int. Soc. Opt. Eng.* **9153** (2014) 91531P, [[arXiv:1407.2973](#)].
- [95] E. Calabrese et al., *Precision Epoch of Reionization studies with next-generation CMB experiments*, *JCAP* **08** (2014) 010, [[arXiv:1406.4794](#)].
- [96] **Simons Observatory** Collaboration, P. Ade et al., *The Simons Observatory: Science goals and forecasts*, *JCAP* **02** (2019) 056, [[arXiv:1808.07445](#)].
- [97] **CMB-S4** Collaboration, K. N. Abazajian et al., *CMB-S4 Science Book, First Edition*, [[arXiv:1610.02743](#)].
- [98] L. Amendola et al., *Cosmology and fundamental physics with the Euclid satellite*, *Living Rev. Rel.* **21** (2018), no. 1 2, [[arXiv:1606.00180](#)].
- [99] **LSST Dark Energy Science** Collaboration, R. Mandelbaum et al., *The LSST Dark Energy Science Collaboration (DESC) Science Requirements Document*, [[arXiv:1809.01669](#)].
- [100] **DESI** Collaboration, A. Aghamousa et al., *The DESI Experiment Part I: Science, Targeting, and Survey Design*, [[arXiv:1611.00036](#)].
- [101] D. Baumann, A. Nicolis, L. Senatore, and M. Zaldarriaga, *Cosmological Non-Linearities as an Effective Fluid*, *JCAP* **07** (2012) 051, [[arXiv:1004.2488](#)].
- [102] J. J. M. Carrasco, M. P. Hertzberg, and L. Senatore, *The Effective Field Theory of Cosmological Large Scale Structures*, *JHEP* **09** (2012) 082, [[arXiv:1206.2926](#)].
- [103] H. Gil-Marín et al., *The clustering of galaxies in the SDSS-III Baryon Oscillation Spectroscopic Survey: RSD measurement from the LOS-dependent power spectrum of DR12 BOSS galaxies*, *Mon. Not. Roy. Astron. Soc.* **460** (2016), no. 4 4188–4209, [[arXiv:1509.06386](#)].
- [104] G. D’Amico, L. Senatore, and P. Zhang, *Limits on w CDM from the EFTofLSS with the PyBird code*, *JCAP* **01** (2021) 006, [[arXiv:2003.07956](#)].